# Partition coefficient of phosphorus between liquid metal and silicate melt with implications for the Martian magma ocean

Tingting Gu[a,*], Vincenzo Stagno[b], Yingwei Fei[c]

[a] *Gemological Institute of America, 50 W 47th ST, New York, NY 10036, USA*
[b] *Department of Earth Sciences, Sapienza University of Rome, 00185, Italy*
[c] *Geophysical Laboratory, Carnegie Institution of Washington, Washington, DC 20015, USA*

## ABSTRACT

Phosphorus in Martian mantle is believed to be five to ten times more abundant than in Earth's mantle, and the distribution of this essential ingredient for life between different deep reservoirs is critical for understanding the habitability of the red planet. In this study, we investigated the behavior of phosphorus in a Martian magma ocean scenario, and measured the partition coefficient of phosphorus ($D_P$) between liquid metal and silicate melt within the pressure range of 3–8 GPa, temperatures between 1973 and 2173 K and oxygen fugacity ranging from $-1.5$ to $\sim -2.5$ as normalized to the iron-wüstite oxygen buffer. Our results show $D_P$ increasing with pressure but decreasing with temperature. A decrease of oxygen fugacity has a negative effect on $D_P$. The moderately siderophile character of phosphorus indicates that the Martian core might be an important reservoir of phosphorous. Based on our experimental results and phosphorus abundance in Martian mantle and bulk Mars, a minimum pressure of 5.8–10.4 GPa is estimated at the base of Martian magma ocean or during the impact melting if a contribution from the late accretion scenario is taken into account. The shallow Martian magma ocean would avail the preservation of volatiles after the rapid solidification of the planet.

## 1. Introduction

Phosphorus is a fundamental element in genetic materials (e.g. DNA and RNA) and lipid membranes, and plays essential role in biochemical energy (e.g. the adenosine triphosphate, ATP, molecule) and metabolism (Westheimer, 1987). The distribution of this biochemically important element during the core segregation and magma differentiation of Mars' interior is fundamentally important for understanding the earliest conditions that would have ultimately led to the advent of biology of this planet. Phosphorus was detected in Martian soils and rocks by the Mars Exploration Rovers through alpha particle X-ray spectrometry (Gellert et al., 2006; Ming et al., 2008), which indicated five to ten times more abundant phosphorus in Martian mantle than in Earth. As volatile element, the concentration of phosphorus in the Solar Nebula increases with distance from the Sun according to models of nebular differentiation (Dreibus and Wänke, 1985; Lewis, 1972). Therefore, the bulk phosphorus content of Mars is predicted to be higher than Earth during its initial accretion. The availability of this essential element for life on Mars increases the possibility of abiogenesis on the planet.

Differentiation from magma ocean scenario can be considered as the initial stage that affects the distribution of volatiles between the interior of a planet and its surface, and possibly the formation of a steam atmosphere and the development of life (Elkins-Tanton, 2008). Mars is considered an early-formed planet with a short period of magma ocean scenario lasted only a few tens of millions of years. Unradiogenic initial Hf-isotope compositions of zircons from NWA 7034 Martian regolith breccia indicate a primordial crust formed no later than 4547 Myr ago. As the formation of crust represents the last stage of planetary differentiation, a rapid magma ocean crystallization less than 20 Myr was proposed (Bouvier et al., 2018). Isotope signatures of Martian meteorites such as $^{87}Rb–^{87}Sr$, $^{129}I–^{129}Xe$, $^{187}Re–^{187}Os$, $^{235}U–^{207}Pb$, indicate that Mars accreted rapidly and differentiated into atmosphere, mantle and core at an early stage (Halliday et al., 2001). $^{142}Nd/^{144}Nd$ and $^{182}W/^{184}W$ ratios narrow down the time of Martian magma ocean to $13 \pm 2$ Myr of the origin of the Solar System (Kleine et al., 2002). $^{147}Sm/^{144}Nd$ isotope data yield an age of formation of the Martian basaltic meteorite source regions of $4504 \pm 6$ Myr (Borg et al., 2016) indicating that a stage of protracted accretion or late giant impact could be necessary to sustain a late accretional heating. Martian ancient geochemical features are preserved due to the lack of ongoing plate tectonic process, which inhibits the large-scale homogenization and

* Corresponding author.
  *E-mail address:* gtt.pku@gmail.com (T. Gu).

cycling of volatile species from the interior to the surface in contrast with planets like Earth. Therefore, element distribution features of current observation could be linked closely to Martian differentiation process from its early magma ocean scenario and the possible late giant impact event. Knowledge of the metal-silicate partition coefficient of phosphorus provides critical constraints of Martian early history.

The close association of phosphorus with Fe and Ni of minerals found in meteorites, such as schreibersite (Clarke Jr et al., 1981), allabogdanite (Britvin et al., 2002), and perryite (Okada et al., 1991), along with their stability at high pressure and temperature (Scott et al., 2007; Lehner et al., 2010; Britvin et al., 2019) is natural evidence of the possible occurrence of Fe-Ni phosphides components in planetary cores. By differentiation processes during magma ocean or Solar Nebula condensation, phosphorus might have alloyed with iron and sink into the core as its major reservoir. The structural stability, phase diagrams of iron-phosphorus alloys under high pressures have been widely studied to date (Dera et al., 2008; Gu et al., 2011, 2013, 2014, 2016; Stewart and Schmidt, 2007). However, an experimental investigation of metal-silicate partitioning is needed to model the abundance of phosphorus in planetary core.

The fate of phosphorus in Mars' interior would depend on its partitioning between metal and silicate liquids during core segregation. Currently available experimental studies on the partition coefficient of phosphorus between metal and silicate melts were carried out using lunar basaltic (Steenstra et al., 2017) or terrestrial basaltic composition (Hillgren et al., 1996; Righter et al., 2009, 2010, 2011; Schmitt et al., 1989; Siebert et al., 2011; Steenstra et al., 2017) as starting materials, while the experiments with compositions and conditions comparable to Martian early magma ocean are rather limited. Here we mimic the phosphorus partition conditions during Mars' early magma ocean with the composition of a model silicate mantle (Dreibus and Wänke, 1985). We report the phosphorus partition coefficient between metallic and silicate melts at pressures of 3–8 GPa and temperatures between 1973 and 2173 K. The obtained data were used to estimate the phosphorus content of the mantle and core with implications for the fate of this life essential element in Martian early history.

## 2. Experimental methods

The starting material was prepared from an oxides mixture with bulk composition similar to the proposed mantle composition of Mars (Dreibus and Wänke, 1985; Table 1). After mixing, grinding, and drying for 24 h at 100 °C, the starting material was stored into a furnace and heated to 1373 K in a reduced atmosphere (IW + 1) using a gas mixture of $CO_2$ and CO (27:73 volume ratio) for 24 h to reduce all iron to $Fe^{2+}$. Then, 5 wt% $Fe_3P$ powder (Alfa Aesar company, purity of 99.5%) was added to the starting mixture.

Experiments were conducted with two-stage multi-anvil presses available at the Geophysical Laboratory of the Carnegie Institution of Washington (Washington, DC, USA). For experiments at 3 and 6 GPa, 18/11 assemblages (Corgne et al., 2007) were used in a 1500-ton press at GL. We casted MgO-based ceramic (Ceramacast 584, Aremco Products, Inc.) into octahedron for pressure medium and used $ZrO_2$ tube as thermal insulator. Cylindrical graphite was used as furnace and a coaxial $W_{5\%}Re/W_{26\%}$ tungsten-rhenium thermocouple (C-type) was used for temperature measurements. Pressure was calibrated according to quartz/coesite transition at 3.2 GPa and 1200 °C (Bohlen and

Boettcher, 1982), garnet/perovskite transition at 5.9 GPa and 1200 °C (Yagi et al., 1987), coesite/stishovite at 8.7 GPa and 1000 °C (Susaki et al., 1985) and 9.2 GPa and 1200 °C, respectively (Zhang et al., 1996). Error on the pressure calibration is generally low within 0.2–0.3 GPa. The height of the sample chamber is less than 2.5 mm, and the axial temperature gradient is estimated within 20 °C (van Westrenen et al., 2003). Single crystal olivine was employed as sample container to prevent contamination from using either metal (Fe, Mo, Re) or graphite or BN capsules. The average composition of the olivine was determined as 51.41 wt% MgO, 41.31 wt% $SiO_2$, 7.40 wt% FeO, 0.44 wt% NiO. Each olivine capsule was dried in the oven at 383 K for at least 3 h before experiments. For experiments at 8 GPa, we used the 10/5 cell assembly described by Bertka and Fei (1997).

For each experiment, we first increased the hydraulic pressure to the target value, and then heated the sample at a rate of 100 °C/min by controlling the power (in Watts). The sample was, then, quenched by turning off the power. To minimize the potential contamination by element diffusion from the capsule material due to the high temperature, we run very short experiments of about 1 min. Longer runs were performed to evaluate the effect of duration on results of partition coefficient, like in experiments at 1973 K and 3 GPa for 1 min, 15 min, 20 min, and 36 min (Fig. 1).

After quenched, all samples were recovered, placed in epoxy resin and polished with SiC abrasive papers. To prevent possible reactions of $Fe_3P$ with water, diamond powder (0.25–6 μm in size) with oil lubricant was used for the final polishing, followed by accurate cleaning of the samples using ethanol. The samples were analyzed with an electron microprobe (JEOL 8900 L) at 15 kV acceleration voltage and 15 nA current. Analyses of the silicate melt were obtained by averaging the chemical composition of 20–40 data points within an area of $\sim 25 \times 25\ \mu m^2$. Those analyses showing an excess of W and Re likely due to contamination during the experiment from the cell assembly were not used for the purpose of this study. The carbon content of the metallic liquid was not measured due to difficulties of quantifying carbon content with electron probe without a proper calibration.

## 3. Results

Selected electron back-scattered images of the quenched run products are shown in Fig. 2a-d. Table 2 shows the experimental conditions along with the recovered phase assemblage. All run products exhibit coexisting silicate melts and liquid metal segregated into two discrete phases with sharp interface, surrounded by elongated olivine that due to the skeletal texture we interpreted as quench crystal. At 3 GPa, silicate liquids quenched to glasses with tabular and skeletal olivine crystals. The liquid metal is trapped by silicate liquids and form blebs $\sim 25\ \mu m$ of diameter at $\sim 1973$ K (Fig. 2a). Similar textures can be observed for run product quenched from 4.5 GPa, while the diameter of liquid metal appears $\sim 40\ \mu m$ at higher temperature (2073 K; Fig. 2b). The silicate glass matrix appears interconnected with dihedral angles above 60° at 2073 K. At 6 GPa, the silicate liquids show a clear interconnected network with little skeletal olivine crystals in between (Fig. 2c-d). Metallic liquids start to aggregate at 1973 K, and small metal blebs merge into one bigger bleb with double bubble shape or oval shape (Fig. 2c). The dihedral angles are generally above 120°. At 2073 K, several metal blebs above 30 μm are surrounded by silicate liquids. As shown in Fig. 2d, the silicate melts are composed by

**Table 1**
Martian mantle bulk composition and the simplified starting composition used in this study (wt%). Composition by Taylor (2013) was listed for comparison.

| $SiO_2$ | MgO | FeO | $Al_2O_3$ | CaO | $P_2O_5$ | $Na_2O$ | $TiO_2$ | $Cr_2O_3$ | MnO | $K_2O$ | Reference |
|---|---|---|---|---|---|---|---|---|---|---|---|
| 44.40 | 30.20 | 17.9 | 3.02 | 2.45 | 0.16 | 0.5 | 0.14 | 0.76 | 0.46 | 0.03 | Dreibus and Wänke, 1985 |
| 43.7 | 30.5 | 18.1 | 3.04 | 2.43 | 0.15 | 0.53 | 0.14 | 0.73 | 0.44 | 0.04 | Taylor, 2013 |
| 45.09 | 30.67 | 18.18 | 3.07 | 2.45 | – | 0.51 | – | – | – | – | This study |
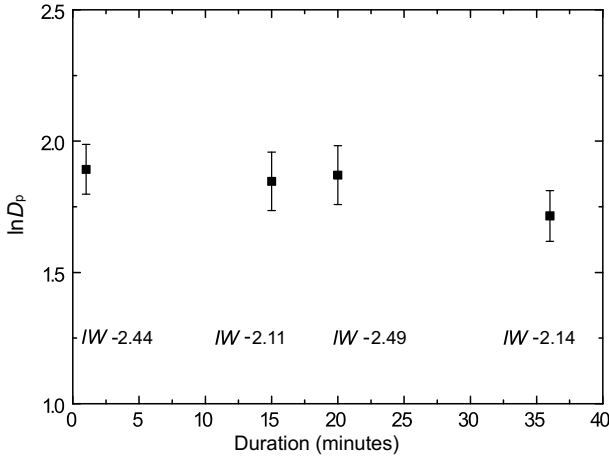
**Fig. 1.** Metal-silicate partitioning as a function of run duration performed at 3 GPa, 1973 K, and between IW-2.11 and IW-2.49.

interconnected glasses with fine skeletal textures on the up-left corner and mixed with tabular olivine crystal on the down-right corner. The different textures might be caused by thermal gradient. The finer texture is caused by a faster cooling; since the cooling time of the whole sample is equal, the area with finer textures would experience higher temperature than the area with coarse tabular textures. We observed a preferred concentration of metal blebs in up-left area of Fig. 2d with fine interconnected glasses, indicating the metallic liquids move to the high-temperature area along thermal gradient.

Chemical compositions of the quenched silicate melts and metallic liquids are listed in Tables 3 and 4. The overall Mg/Si ratios in the silicate melts of the products obtained in olivine capsules are generally consistent with the starting value. While the Mg contents are significantly higher in those runs performed in MgO capsules (PR985,

PR986). In addition, the Fe content also shows a lower concentration in those run products. Al concentration is higher in silicate products run with MgO capsules (PR985, PR986) or at higher temperature (M1223). Trace amounts of Ni were detected in the silicate melts introduced by the olivine capsules. We noted low totals from the chemical analyses of all metallic phases (Table 4), which might be due to the presence of carbon diffused from the graphite heater through indistinctly both olivine and MgO capsules. However, restricted by C-coating and reliable standard, carbon content was not measured here, although the content (between 3 and 6 wt%) is somehow lower than what proposed by Siebert et al. (2011) at saturation levels when graphite capsules are employed. Phosphorus concentration in silicate melts decreases from 0.78 wt% to 0.37 wt% with pressure increasing from 3 GPa to 8 GPa, at 1973 K within the same duration of the run. Meanwhile, at each pressure condition, its concentration increases with temperature from 1973 K to 2173 K. In metallic liquids, phosphorus concentration increases both with temperature and pressure.

Metal/silicate partition coefficients of phosphorus ($D_P$) at different pressures and temperatures were calculated as (mol.% element in metallic liquid)/(mol.% element in silicate melt), and the results are listed in Table 2. The variation of ln $D_P$ as a function of temperature at each pressure is plotted in Fig. 4. Within the same duration of the runs, ln$D_P$ generally shows an increasing trend with pressure but decreasing with temperature. Smaller values observed at 3 GPa and 1973 K refers to a longer heating time.

Oxygen fugacity ($fO_2$) of each run was calculated according to Li and Agee (1996) as:

$$Fe + \frac{1}{2}O_2 = FeO \tag{1}$$

$$\log fO_2 = \log fO_2(IW) + 2\log a_{FeO}^{silicate\ melt} - 2\log a_{Fe}^{metallic\ liquid} \tag{2}$$

$$\Delta IW = 2\log\left(\frac{a_{FeO}^{silicate\ melt}}{a_{Fe}^{metal\ liq}}\right) = 2\log\left(\frac{x_{FeO}^{silicate\ melt}}{x_{Fe}^{metal\ liq}}\right) + 2\log\left(\frac{\gamma_{FeO}^{silicate\ melt}}{\gamma_{Fe}^{metal\ liq}}\right) \tag{3}$$
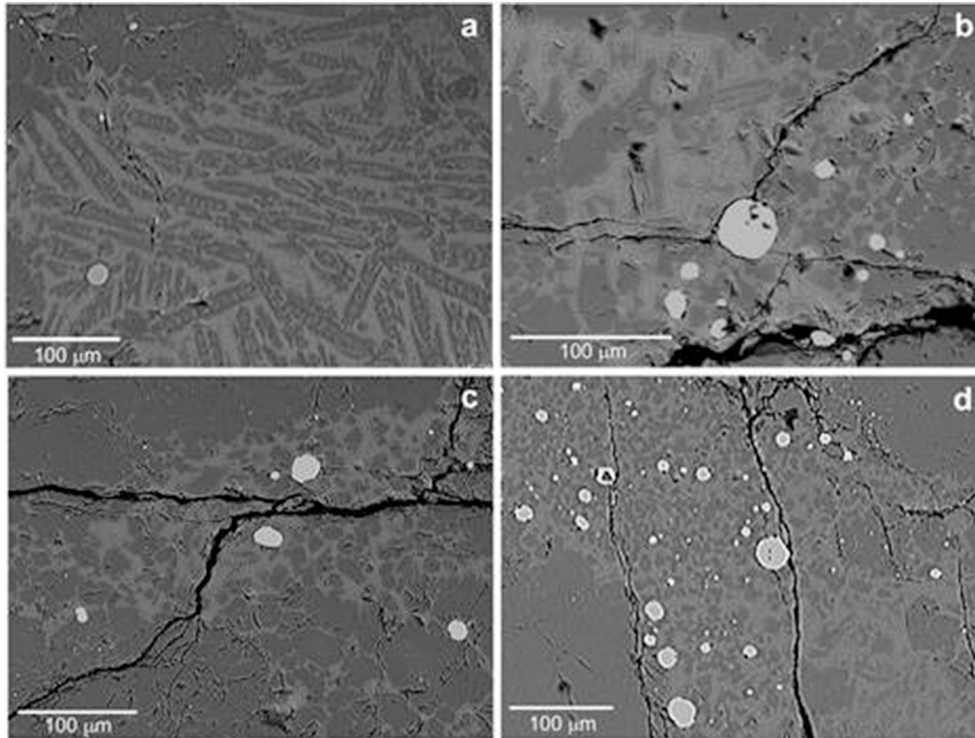


**Fig. 2.** Back-scattered electron images of quenched samples. (a) Run product at 3 GPa and 1973 K showing silicate melts with metallic spheres and skeletal olivine crystals (b) Sample synthesized at 4.5 GPa and 2073 K (run PR1040) (c) Sample synthesized at 6 GPa and 1973 K (run PR1014) (d) Sample synthesized at 6 GPa and 2073 K (run PR1015).

**Table 2**

Experimental conditions and final products of each run along with the calculated $f\mathrm{O}_2$ (normalized to IW) and phosphorus partition coefficient ($\ln D$). Numbers in parentheses are uncertainties given as two standard deviations.

| Run | $P$(GPa) | $T$(K) | Time (min) | Phase assemblage | ΔIW | $lnD$ |
|---|---|---|---|---|---|---|
| M1218 | 3 | 1973 | 1 | Silicate melts, metallic liquids, skeletal olivine crystals | −2.44 | 1.89(9) |
| M1214 | 3 | 1973 | 15 | Silicate melts, metallic liquids, olivine crystals | −2.11 | 1.85(11) |
| PR1023 | 3 | 2073 | 1 | Silicate melts, metallic liquids, skeletal olivine crystals | −1.74 | 2.12(12) |
| PR985 | 3 | 1973 | 20 | Silicate melts, metallic liquids, olivine crystals | −2.49 | 1.87(11) |
| PR986 | 3 | 1973 | 36 | Silicate melts, metallic liquids, olivine crystals | −2.14 | 1.72(10) |
| PR1048 | 4.5 | 1973 | 1 | Silicate melts, metallic liquids, skeletal olivine crystals | −1.99 | 2.77(12) |
| PR1040 | 4.5 | 2073 | 1 | Silicate melts, metallic liquids, skeletal olivine crystals | −1.77 | 2.55(17) |
| PR1014 | 6 | 1973 | 1 | Silicate melts, metallic liquids, skeletal olivine crystals | −1.95 | 3.17(10) |
| PR1015 | 6 | 2073 | 1 | Silicate melts, metallic liquids, skeletal olivine crystals | −1.81 | 2.92(11) |
| M1223 | 8 | 2173 | 1 | Silicate melts, metallic liquids, skeletal olivine crystals | −1.74 | 2.91(13) |

where $a_{\mathrm{FeO}}^{\mathrm{silicate\ melt}}$ is the activity of FeO molar fraction in silicate melt, and $a_{\mathrm{Fe}}^{\mathrm{metal\ liq}}$ is the activity of Fe molar fraction in the liquid metal alloy. For experiments where the liquid metal alloy is mostly made of Fe, we assumed that $\gamma_{\mathrm{Fe}}^{\mathrm{metal\ liq}}$ is 1 and the activity of Fe in the metal liquid is, therefore, equal to its mole fraction. The calculated $f\mathrm{O}_2$ was normalized to IW buffer, and listed in Table 2. Our data fall in the range of $-2.5 < \log f\mathrm{O}_2\ (\Delta\mathrm{IW}) < -1.5$. Due to the possible dissolution of carbon into the alloy, $\gamma_{\mathrm{Fe}}^{\mathrm{metal}}$ is expected to decrease causing the actual $\log f\mathrm{O}_2$ being 0.3 log units higher than C-free runs.

Using an exchange reaction, the effect of $f\mathrm{O}_2$ can be intrinsically taken into account. The equilibrium constant of the exchange reaction is related to the Gibbs free energy of formation, $\Delta G_{P,T}^0$ from pure oxides and metals by

$$RT \ln DP = -\Delta G^0 = -\Delta H^0 + T\Delta S^0 - \int_{P^0}^{P} \Delta V \cdot \mathrm{d}P \qquad (4)$$

where $R$ is the gas constant, $\Delta H^0$ and $\Delta S^0$ are the standard state enthalpy and entropy changes, and $\Delta V$ is the molar volume change of the exchange reaction.

By assuming a constant volume change, the expression, $\ln D$ can be related with temperature, pressure, and oxygen fugacity with the following equation (Righter et al., 1997):

$$\ln D = a \ln f\mathrm{O}_2 + b/T + cP/T + d\mathrm{NBO}/T + f \qquad (5)$$

where $a$, $b$, $c$, $d$ and $f$ are fitting terms. $a$ term is related to the elements in the silicate melt, $d$ term is related to the ratio of non-bridging oxygens, while $b$, $c$, and $f$ terms result from the expansion of the free energy term (Eq. (4)). $T$ is the temperature in Kelvin and $P$ the pressure in GPa.

We obtained parameters of $a = -0.404$ ($\pm 0.5$), $b = -17{,}445$ ($\pm 3784$), $c = 579$ ($\pm 144$), $d = -0.725$ ($\pm 0.47$), $f = -3.15$ ($\pm 3.7$), yielding $R^2$ value of 0.87, and the calculated data are within acceptable error (Fig. 3). We also compared our results with previous data obtained from basaltic compositions at 1.5–7 GPa and 1575–2025 K (Righter et al., 1997), and at ambient pressure from 1300 to 1900 K (Newsom and Drake, 1983; Schmitt et al., 1989). Besides, we also compared the more recent data collected at 1 GPa and 1750–2200 K (Righter et al., 2010), 0.5–18 GPa and 1873–2873 K (Siebert et al., 2011), and 1.5 GPa and 1683–1883 K (Steenstra et al., 2017), which yield a larger value of $a$ parameter ($a = -1.120$) than our study (Fig. 3). However, in previous studies, the content of other siderophile elements were parameterized, yet in our study, we were not able to parameterize the effect of elements (such as carbon) on $f\mathrm{O}_2$ here. Thus we observed a relatively smaller $a$ value compared with previous studies (e.g., $a = -0.677$; Righter et al., 2009), which reflects both the valence state of phosphorus as well as the possible effect of other elements in our system. The discrepancy in these parameters yielded from previous data done at different conditions indicates that the pressure, temperature and melt compositions have non-negligible effects on phosphorus partition coefficient. Indeed, previous studies also shown that CaO and MgO content of the silicate melt has notable effects on $D_{\mathrm{P}}$ (Siebert et al., 2011; Steenstra et al., 2017).

## 4. Discussions

Compared with partition coefficient of phosphorus, we also found that the value of partition coefficient of nitrogen ($D_{\mathrm{N}}$) from literature is comparable to $D_{\mathrm{P}}$. Fig. 5 shows $D_{\mathrm{P}}$ and $D_{\mathrm{N}}$ (Dalou et al., 2017; Kadik et al., 2011, 2013; Li et al., 2016; Roskosz et al., 2013) as a function of oxygen fugacity. Despite the pressure and temperature effects, $D_{\mathrm{P}}$ is slightly higher than $D_{\mathrm{N}}$ at the same oxygen fugacity. According to previous studies, oxygen fugacity generally has a positive effect on $D_{\mathrm{N}}$. In contrast, an opposite trend was observed for $D_{\mathrm{P}}$ according to previous studies (Hillgren et al., 1996; Righter et al., 2010; Siebert et al., 2011; Steenstra et al., 2017; Newsom and Drake, 1983; Schmitt et al., 1989), with $D_{\mathrm{P}}$ decreasing under higher oxygen fugacity at ambient pressure. Since the range of $f\mathrm{O}_2$ in our study is relatively narrow, the influence of redox conditions on $D_{\mathrm{P}}$ in our study is not distinguishable. However,

**Table 3**

Average composition of silicate melts (wt%) of each run. Numbers in parentheses are uncertainties given as two standard deviations.

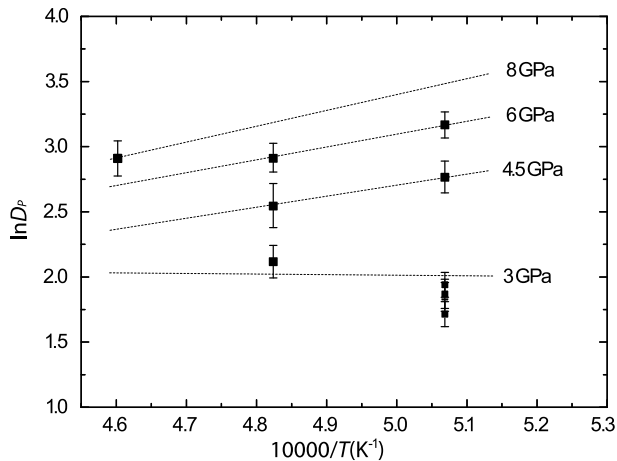| Run | $SiO_2$ | MgO | FeO | $Al_2O_3$ | CaO | $P_2O_5$ | $Na_2O$ | NiO | nbo/t | Tot. |
|---|---|---|---|---|---|---|---|---|---|---|
| M1218[a] | 34.37(39) | 48.86(74) | 8.70(81) | 6.56(11) | 1.13(6) | 0.78(6) | 0.24(6) | – | 2.57 | 100.53 |
| M1214[a] | 46.11(53) | 38.69(96) | 11.88(78) | 2.85(23) | 0.22(9) | 0.83(7) | 0.88(7) | – | 1.29 | 101.48 |
| PR1023 | 43.63(48) | 30.13(77) | 16.46(1.13) | 5.63(21) | 2.18(12) | 1.03(10) | 0.39(3) | 0.03(2) | 0.88 | 99.48 |
| PR985[a] | 33.34(87) | 45.27(1.14) | 7.78(69) | 10.03(16) | 1.80(11) | 1.38(12) | 0.27(3) | – | 2.21 | 99.87 |
| PR986[a] | 30.77(76) | 40.69(1.03) | 10.95(71) | 11.70(23) | 3.24(10) | 3.30(25) | 0.91(5) | – | 2.14 | 101.56 |
| PR1048 | 46.73(38) | 37.00(87) | 12.95(85) | 1.91(12) | 1.06(11) | 0.44(4) | 0.19(4) | 0.01(1) | 1.24 | 100.28 |
| PR1040 | 45.08(55) | 32.37(64) | 15.13(1.24) | 3.62(13) | 1.73(23) | 0.86(12) | 0.26(7) | 0.01(1) | 1.00 | 99.06 |
| PR1014 | 45.12(48) | 35.38(85) | 13.28(1.05) | 3.89(18) | 1.22(29) | 0.37(3) | 0.19(3) | 0.03(1) | 1.12 | 99.47 |
| PR1015 | 45.28(84) | 33.12(63) | 14.93(1.17) | 3.08(20) | 1.95(24) | 0.69(6) | 0.28(4) | – | 1.08 | 99.32 |
| M1223 | 37.98(96) | 33.39(89) | 15.49(1.29) | 10.05(46) | 1.80(23) | 0.66(7) | 0.17(3) | 0.25(2) | 0.97 | 99.83 |

[a] MgO capsules were used for those runs.

**Table 4**

Average composition of metallic liquids (wt%) of each run. Numbers in parentheses are uncertainties given as two standard deviations.
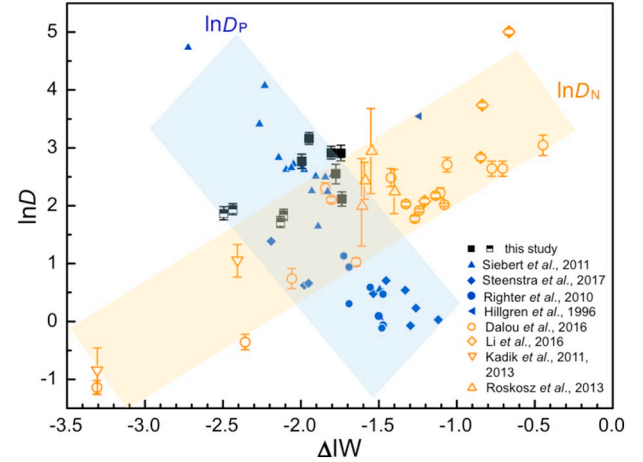
| Run | Fe | Ni | Mg | Si | Al | P | O | Tot. |
|---|---|---|---|---|---|---|---|---|
| M1218[a] | 93.94(1.06) | – | 0.03(1) | 0.06(2) | – | 1.89(3) | – | 95.92 |
| M1214[a] | 92.81(1.09) | – | 0.06(2) | 0.08(3) | 0.01(1) | 2.03(5) | 0.61(4) | 95.62 |
| PR1023 | 90.15(1.15) | 2.55(12) | 0.02(1) | 0.04(2) | 0.08(2) | 3.55(9) | 0.28(2) | 96.67 |
| PR985[a] | 92.31(1.28) | – | 0.05(2) | 0.04(2) | 0.21(2) | 3.37(8) | – | 95.98 |
| PR986[a] | 89.34(1.17) | – | 0.04(2) | 0.05(2) | 0.10(3) | 7.18(16) | – | 96.71 |
| PR1048 | 87.91(1.09) | 1.70(10) | 0.03(1) | 0.01(1) | – | 2.68(8) | 0.42(3) | 96.92 |
| PR1040 | 85.89(94) | 3.60(11) | 0.04(2) | 0.06(2) | 0.23(2) | 4.53(10) | 0.55(9) | 94.93 |
| PR1014 | 88.66(1.07) | 2.54(8) | 0.06(2) | 0.04(2) | – | 3.50(6) | 0.30(10) | 95.10 |
| PR1015 | 89.18(1.24) | 1.43(7) | 0.06(3) | 0.04(2) | 0.10(2) | 5.33(12) | 0.47(3) | 96.63 |
| M1223 | 84.32(1.32) | 5.39(8) | 0.08(3) | 0.07(3) | 0.12(3) | 4.97(13) | 0.73(6) | 95.68 |

[a] MgO capsules were used for those runs.
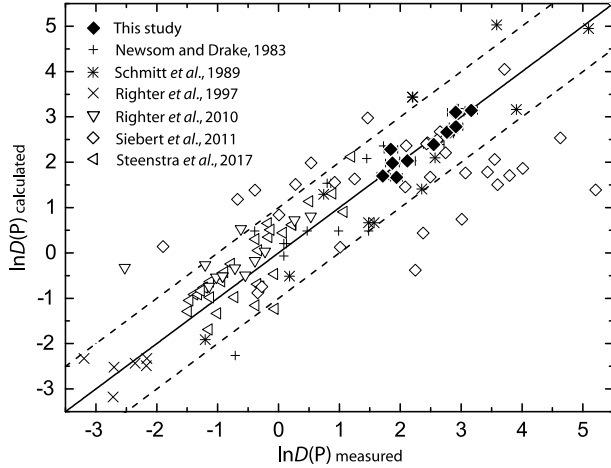


**Fig. 3.** Comparison between calculated and measured values of $\ln D_P$ from this study and previous studies. Dashed lines are $\pm 1\sigma$ error on the regressions. Solid diamonds (this study) are using equation of the form $\ln D = a \ln f O_2 + b/T + cP/T + d\ nbo/t + f$ where $a = -0.404\ (\pm 0.5)$, $b = -17{,}445\ (\pm 3784)$, $c = 579\ (\pm 144)$, $d = -0.725\ (\pm 0.47)$, $f = -3.15\ (\pm 3.7)$, $R^2 = 0.87$. Open symbols (Righter et al., 2010; Siebert et al., 2011; Steenstra et al., 2017) are compared where $a = -1.120\ (\pm 0.15)$, $b = -77{,}076\ (\pm 8442)$, $c = 787\ (\pm 97)$, $d = -0.604\ (\pm 0.15)$, $f = 1.048\ (\pm 1.9)$, $R^2 = 0.74$. Calculated results for previous data done at ambient pressure are obtained with equation $\ln D = a \ln f O_2 + b/T + c$, where pressure is not considered, and $a$, $b$ is $-1.191$, $-102{,}300$, respectively. $c$ is 33.94 for crosses (Newsom and Drake, 1983), while $c$ is modified to 33.54 for stars (Schmitt et al., 1989) and rotated crosses (Righter et al., 1997) to achieve better fitting.
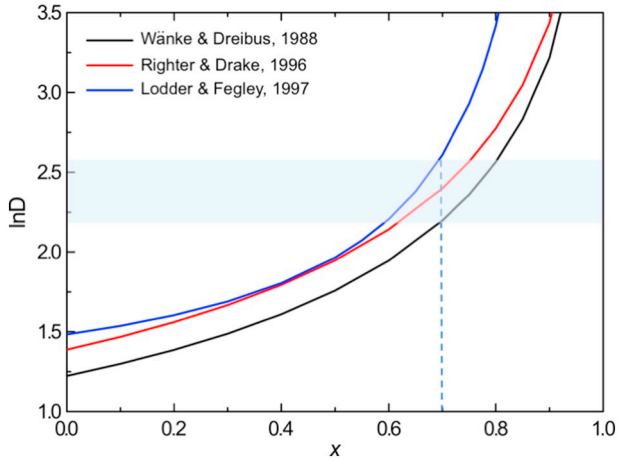


**Fig. 5.** Phosphorus partition coefficients between melted metal and silicate ($D_P$) in current study and previous studies (Hillgren et al., 1996; Righter et al., 2010; Siebert et al., 2011; Steenstra et al., 2017) as a function of oxygen fugacity regardless of pressure and temperature. Nitrogen partition coefficients between melted metal and silicate ($D_N$) are also plotted for comparison (Kadik et al., 2011, 2013: 1.5 GPa, 1400 °C, 4 GPa, 1550 °C; Roskosz et al., 2013: 1.8–14.8 GPa, 2200–2500 °C; Li et al., 2016: 1.5–7 GPa, 1600–1800 °C; Dalou et al., 2017: 1.2–3 GPa, 1400–1600 °C). Blue and yellow shadows are guides for the eyes for the variation of $D_P$ and $D_N$ as a function of oxygen fugacity. (For interpretation of the references to colour in this figure legend, the reader is referred to the web version of this article.)



**Fig. 4.** Partition coefficient $\ln D_P$ for phosphorus between molten metal and silicate as a function of inverse temperature (10,000/$T$) in Kelvin. Dashed lines are guides for the eyes.

comparing the data obtained from experiments done with the same capsule materials, $fO_2$ tends to have a negative effect on $D_P$ (Fig. 5). The higher content of Mg in silicate liquid introduced by MgO capsules yields a larger ratio of non-bridging oxygens than that of a silicate melts in single olivine capsules (Table 3), which could affect $D_P$ and its relationship with $fO_2$. Although both phosphorus and nitrogen are moderate siderophile elements, the opposite effect of $fO_2$ on $D_P$ and $D_N$ would influence their behaviors during the core formation scenario if the oxygen fugacity were relatively low. At low oxygen fugacity, phosphorus would preferentially be incorporated in planetary cores while nitrogen would be more dissolvable into silicates. Detection of nitrogen-bearing compounds in Martian soil (Stern et al., 2015) implies an appropriate initial condition that could sustain nitrogen in Martian lithosphere. Migration of nitrogen and phosphorus would have important implication for the possibility of the past and present life on this planet.

With values of phosphorus partition coefficients between liquid metal and silicates, we can assess the accretion conditions during Martian differentiation. The relationship of siderophile element abundances, liquid metal/liquid silicate, solid metal/liquid silicate partition coefficients, and the solid/melt silicate fraction of the planet can be parameterized using the following equation (Righter and Drake, 1996):

**Fig. 6.** The relationship of phosphorus metal-silicate partition coefficient as a function of silicate fraction of Mars ($x$) based on Eq. (4). The red and black lines are based on phosphorus abundance in Martian mantle ($C_{LS}^i$) of 594 ppm (Righter and Drake, 1996) and 700 ppm (Wänke and Dreibus, 1988) with bulk phosphorus concentration in Mars ($C_{bulk}^i$) of 2379 ppm. The blue line is based on phosphorus abundance in Martian mantle ($C_{LS}^i$) of 742 ppm, and in bulk Mars ($C_{bulk}^i$) of 1100 ppm (Lodders and Fegley, 1997). Dashed line indicates the estimated silicate fraction ($x$) at the magma ocean scenario and the shadow indicates the inferred phosphorus partition coefficient at this stage. (For interpretation of the references to colour in this figure legend, the reader is referred to the web version of this article.)

$$C_{bulk}^i$$
$$= x[C_{LS}^i[p + (1 - p)D_{SS/LS}^i] + (1 - x)$$
$$[C_{LS}^i[mD_{LM/LS}^i + (1 - m)D_{SM/LS}^i]] \tag{6}$$

where $x$ is silicate fraction of the planet; $p$ is fraction of the silicate that is molten; and $m$ is fraction of the metal that is molten; $C_{LS}^i$, $C_{bulk}^i$ are concentrations of siderophile elements in the silicate and bulk portions of the planet; $D_{LM/LS}^i$ is the liquid metal/liquid silicate partition coefficient, and $D_{SM/LS}^i$ is the solid metal/liquid silicate partition coefficient, and $D_{SS/LS}^i$ is the solid silicate/liquid silicate partition coefficient.

In a magma ocean-like scenario, $p$ and $m$ in the Eq. (6) are 1, thus Eq. (6) can be further simplified as:

$$C_{bulk}^i = xC_{LS}^i + (1 - x)C_{LS}^i D_{LM/LS}^i \tag{7}$$

which means the phosphorus partition coefficient can be determined at each value of silicate fraction of the planet. The concentration of phosphorus in the bulk can be derived from previous data, from 1100 ppm phosphorus in bulk Mars (Lodders and Fegley, 1997) to 1.95 times the bulk concentration of phosphorus in CI, i.e., 2379 ppm (Righter and Drake, 1996; Treiman et al., 1987). The concentration of phosphorus in the silicate mantle is estimated between 594 ppm (Righter and Drake, 1996; Treiman et al., 1987) to 700 ppm (Wänke and Dreibus, 1988; Taylor, 2013) or 742 ppm (Lodders and Fegley, 1997). With those parameters, the relationship of the phosphorus partition coefficient and the silicate fraction of the planet ($x$) can be plotted in Fig. 6. Based on previous observations, $x = 0.7$ is a reasonable value consistent with geophysical evidence for Martian core (Longhi et al., 1992), which means 70% of the planet is constituted by molten silicate when the magma ocean was formed. The corresponding $\ln D_P$ is from 2.2 to 2.6 according to this model (Fig. 6). The calculated pressure range based on Eq. (4) is 5.8 to 10.4 GPa, giving the temperature from 1900 to 2200 K, and oxygen fugacity from $\Delta$IW–1.5 to $-1$ (Rai and van Westrenen, 2013). The estimated pressure of magma ocean is relatively lower than previous value. Using the calculated siderophile element partition coefficient, the best fit for the depth of Martian magma ocean is corresponding to pressures at 6–9 GPa, 1900–2000 K and the calculated oxygen fugacity is around $\Delta$IW–1.25 (Righter and Drake, 1996). In

this study, we focused on phosphorus partition coefficient and the effect of other elements on $D_P$ was not parameterized here. The content of sulfur in Martian core is restricted by oxygen fugacity, and at $\log fO_2$ of about $\Delta$IW–1, the sulfur content would be lower than 10.5 wt% (Rai and van Westrenen, 2013), while a minimum 7 wt% sulfur was expected (Steenstra and van Westrenen, 2018). Previous experiments showed that higher sulfur content would enhance the partition coefficient of highly siderophile elements Ir, Pt and Re by segregating as sulfur-poor, siderophile element-rich alloys, while decrease the partition coefficient of moderately siderophile elements Ge, W, and P (Jana and Walker, 1997). Therefore, with the presence of sulfur, the partition coefficient of phosphorus would be smaller. Similar effects are observed for carbon in the core (Siebert et al., 2011). However, the carbon content in Martian core is much lower than that of sulfur, which is estimated to be ~1–1.4 wt% (Filiberto et al., 2016; Steenstra and van Westrenen, 2018). The estimated carbon content in the metallic phase is around 4 wt%, which would decrease the partition coefficient of phosphorus. If the carbon content here is not high enough to compensate the decreasing effect on $D_P$ due to sulfur, the estimated pressure of Martian magma ocean at 5.8 to 10.4 GPa would be a lower bound. The core formation process should have deprived highly siderophile elements from the mantle. However, over-abundance of highly siderophile elements in Martian mantle would imply a late accretion scenario (Bottke et al., 2010), and a lull in impact before Late Heavy Bombardment event has been proposed (Bottke and Andrews-Hanna, 2017). In the situation of late giant impact, it would have generated a minimum pressure of 5.8–10.4 GPa during the late stage impact melting (Borg et al., 2016) to match the balance of phosphorus content in Martian mantle.

The partition coefficients indicate a moderately siderophile behavior of phosphorus, which during Martian accretion, would tend to concentrate in Martian core as pressure increases. The high abundance of phosphorus in Martian mantle indicates that Martian core is an important reservoir of this element. Therefore, the iron-phosphorus related compounds would have significant effects on the properties of Martian core (Scott et al., 2007; Gu et al., 2016; Gu et al., 2014; Gu et al., 2011; Davies and Pommier, 2018). The shallow magma ocean or impact melting region on Mars would prevent volatile elements from vast evaporating, leaving volatile-rich materials on the ancient surface of Mars before buried by other regolith. The consistent correlation of phosphorus concentration with sulfur and chlorine in different areas of Martian soil would be resulting from homogenization of phosphate, sulfate, and chloride in a large acidic paleo oceans (Greenwood and Blake, 2006). Besides, it was found that aqueous corrosion of iron phosphides can produce metastable mixture of mixed-valence P-bearing ions that can form key components for metabolism in modern life (Pasek and Lauretta, 2005). Therefore, the chemically active iron-phosphides could have been a significant source for the prebiotic phosphorous in Martian early history.

**References**

Bertka, C.M., Fei, Y., 1997. Mineralogy of the Martian interior up to core-mantle boundary. J. Geophys. Res. 102, 5251–5264.

Bohlen, S.R., Boettcher, A.L., 1982. The quartz ⇌ coesite transformation: a precise determination and the effects of other components. J. Geophys. Res. 87, 7073–7078.

Borg, L.E., Brennecka, G.A., Symes, S.J.K., 2016. Accretion timescale and impact history of Mars deduced from the isotopic systematics of martian meteorites. Geochim. Cosmochim. Acta 175, 150–167. https://doi.org/10.1016/j.gca.2015.12.002.

Bottke, W.F., Andrews-Hanna, J.C., 2017. A post-accretionary lull in large impacts on early Mars. Nat. Geosci. 10, 344–348. https://doi.org/10.1038/ngeo2937.

Bottke, W.F., Walker, R.J., Day, J.M.D., Nesvorny, D., Elkins-Tanton, L., 2010. Stochastic late accretion to earth, the moon, and mars. Science 330, 1527. https://doi.org/10.1126/science.1196874.

Bouvier, L.C., Costa, M.M., Connelly, J.N., Jensen, N.K., Wielandt, D., Storey, M., Nemchin, A.A., Whitehouse, M.J., Snape, J.F., Bellucci, J.J., Moynier, F., Agranier, A., Gueguen, B., Schönbächler, M., Bizzarro, M., 2018. Evidence for extremely rapid magma ocean crystallization and crust formation on Mars. Nature 558, 586–589. https://doi.org/10.1038/s41586-018-0222-z.

Britvin, S.N., Rudashevsky, N.S., Krivovichev, S.V., Burns, P.C., Polekhovsky, Y.S., 2002. Allabogdanite, (Fe,Ni)₂P, a new mineral from the Onello meteorite: The occurrence and crystal structure. Am. Mineral. 87, 1245–1249.

Britvin, S.N., Shilovskikh, V.V., Pagano, R., Vlasenko, N.S., Zaitsev, A.N., Krzhizhanovskaya, M.G., Lozhkin, M.S., Zolotarev, A., Gurzhiy, V.V., 2019. Allabogdanite, the high-pressure polymorph of (Fe,Ni)₂P, a stishovite-grade indicator of impact processes in the Fe–Ni–P system. Sci. Rep. 9 (1), 1047–1048. https://doi.org/10.1038/s41598-018-37795-x.

Clarke Jr., R.S., Appleman, D.E., Ross, D.R., 1981. An Antarctic iron meteorite contains preterrestrial impact-produced diamond and Ionsdaleite. Nature 291, 396–398.

Corgne, A., Wood, B.J., McDonough, W.F., Keshav, S., Fei, Y., 2007. New metal-silicate partition coefficients and constraints on core composition and oxygen fugacity during Earth accretion. Geochim. Cosmochim. Acta 71, A189.

Dalou, C., Hirschmann, M.M., von der Handt, A., Mosenfelder, J., Armstrong, L.S., 2017. Nitrogen and carbon fractionation during core-mantle differentiation at shallow depth. Earth Planet. Sci. Lett. 458, 141–151. https://doi.org/10.1016/j.epsl.2016.10.026.

Davies, C.J., Pommier, A., 2018. Iron snow in the Martian core? Earth Planet. Sci. Lett. 481, 189–200. https://doi.org/10.1016/j.epsl.2017.10.026.

Dera, P., Lavina, B., Borkowski, L.A., Prakapenka, V.B., Sutton, S.R., Rivers, M.L., Downs, R.T., Boctor, N.Z., Prewitt, C.T., 2008. High-pressure polymorphism of Fe₂P and its implications for meteorites and earth's core. Geophys. Res. Lett. 35, L10301. https://doi.org/10.1029/2008GL033867.

Dreibus, G., Wänke, H., 1985. Mars, a volatile-rich planet. Meteoritics 20, 367–381.

Elkins-Tanton, L.T., 2008. Linked magma ocean solidification and atmospheric growth for Earth and Mars. Earth Planet. Sci. Lett. 271, 181–191. https://doi.org/10.1016/j.epsl.2008.03.062.

Filiberto, J., Baratoux, D., Beaty, D., Breuer, D., Farcy, B.J., Grott, M., Jones, J.H., Kiefer, W.S., Mane, P., McCubbin, F.M., Schwenzer, S.P., 2016. A review of volatiles in the Martian interior. Meteorit. Planet. Sci. 51, 1935–1958. https://doi.org/10.1111/maps.12680.

Gellert, R., Rieder, R., Brückner, J., Clark, B.C., Dreibus, G., Klingelhöfer, G., Lugmair, G., Ming, D.W., Wänke, H., Yen, A., Zipfel, J., Squyres, S.W., 2006. Alpha Particle X-Ray Spectrometer (APXS): Results from Gusev crater and calibration report. J. Geophys. Res. 111, E02S05. https://doi.org/10.1038/nature03637. 1–32.

Greenwood, J.P., Blake, R.E., 2006. Evidence for an acidic ocean on Mars from phosphorus geochemistry of Martian soils and rocks. Geology 34, 953. https://doi.org/10.1130/G22415A.1.

Gu, T., Wu, X., Qin, S., Dubrovinsky, L., 2011. In situ high-pressure study of FeP: implications for planetary cores. Phys. Earth Planet. Inter. 184, 154–159. https://doi.org/10.1016/j.pepi.2010.11.004.

Gu, T., Wu, X., Qin, S., McCammon, C., Dubrovinsky, L., 2013. Probing nonequivalent sites in iron phosphide Fe₂P and its mechanism of phase transition. The European Physical Journal B-Condensed Matter 86, 311. https://doi.org/10.1140/epjb/e2013-40086-3.

Gu, T., Fei, Y., Wu, X., Qin, S., 2014. High-pressure behavior of Fe₃P and the role of phosphorus in planetary cores. Earth Planet. Sci. Lett. 390, 296–303. https://doi.org/10.1016/j.epsl.2014.01.019.

Gu, T., Fei, Y., Wu, X., Qin, S., 2016. Phase stabilities and spin transitions of Fe₃(S₁₋ₓPₓ) at high pressure and its implications in meteorites. Am. Mineral. 101, 205–210. https://doi.org/10.2138/am-2016-5466.

Halliday, A.N., Wänke, H., Birck, J.L., Clayton, R.N., 2001. The accretion, composition and early differentiation of Mars. Space Sci. Rev. 96, 197–230.

Hillgren, V.J., Drake, M.J., Rubie, D.C., 1996. High pressure and high temperature metal-silicate partitioning of siderophile elements: the importance of silicate liquid composition. Geochim. Cosmochim. Acta 60, 2257–2263. https://doi.org/10.1016/0016-7037(96)00079-8.

Jana, D., Walker, D., 1997. The influence of sulfur on partitioning of siderophile elements. Geochim. Cosmochim. Acta 61, 5255–5277. https://doi.org/10.1016/S0016-7037(97)00307-4.

Kadik, A.A., Kurovskaya, N.A., Ignat'ev, Y.A., Kononkova, N.N., Koltashev, V.V., Plotnichenko, V.G., 2011. Influence of oxygen fugacity on the solubility of nitrogen, carbon, and hydrogen in FeO-Na₂O-SiO₂-Al₂O₃ melts in equilibrium with metallic iron at 1.5 GPa and 1400°C. Geochem. Int. 49, 429–438. https://doi.org/10.1134/S001670291105003X.

Kadik, A.A., Litvin, Y.A., Koltashev, V.V., Kryukova, E.B., Plotnichenko, V.G., Tsekhonya, T.I., Kononkova, N.N., 2013. Physics of the earth and planetary interiors. Phys. Earth Planet. Inter. 214, 14–24. https://doi.org/10.1016/j.pepi.2012.10.013.

Kleine, T., Münker, C., Mezger, K., Palme, H., 2002. Rapid accretion and early core formation on asteroids and the terrestrial planets from Hf-W chronometry. Nature 418, 952–955. https://doi.org/10.1038/nature00982.

Lehner, S.W., Buseck, P.R., McDonough, W.F., 2010. Origin of kamacite, schreibersite, and perryite in metal-sulfide nodules of the enstatite chondrite Sahara 97072 (EH3). Meteorit. Planet. Sci. 45, 289–303. https://doi.org/10.1111/j.1945-5100.2010.01027.x.

Lewis, J.S., 1972. Metal/silicate fractionation in the solar system. Earth Planet. Sci. Lett. 15, 286–290. https://doi.org/10.1016/0012-821X(72)90174-4.

Li, J., Agee, C.B., 1996. Geochemistry of mantle-core differentiation at high pressure. Nature 381, 686–689. https://doi.org/10.1038/381686a0.

Li, Y., Marty, B., Shcheka, S., Zimmermann, L., Keppler, H., 2016. Nitrogen isotope fractionation during terrestrial core-mantle separation. Geochem. Persp. Let. 138–147. https://doi.org/10.7185/geochemlet.1614.

Lodders, K., Fegley, B., 1997. An oxygen isotope model for the composition of Mars. Icarus 126, 373–394. https://doi.org/10.1006/icar.1996.5653.

Longhi, J., Knittle, E., Holloway, J.R., Wänke, H., 1992. The bulk composition, mineralogy and internal structure of Mars. Mars, Univ. of Arizona press, Tucson.

Ming, D.W., Gellert, R., Morris, R.V., Arvidson, R.E., Brückner, J., Clark, B.C., Cohen, B.A., d'Uston, C., Economou, T., Fleischer, I., Klingelhöfer, G., McCoy, T.J., Mittlefehldt, D.W., Schmidt, M.E., Schröder, C., Squyres, S.W., Tréguier, E., Yen, A.S., Zipfel, J., 2008. Geochemical properties of rocks and soils in Gusev crater, Mars: results of the alpha particle X-ray spectrometer from Cumberland ridge to home plate. J. Geophys. Res. 113, 821–828. https://doi.org/10.1029/2008JE003195.

Newsom, H.E., Drake, M.J., 1983. Experimental investigation of the partitioning of phosphorus between metal and silicate phases - implications for the earth, moon and eucrite parent body. Geochim. Cosmochim. Acta 47, 93–100. https://doi.org/10.1016/0016-7037(83)90093-5.

Okada, A., Kobayashi, K., Ito, T., Sakurai, T., 1991. Structure of synthetic perryite, (Ni,Fe)₈(Si,P)₃. Acta Crystallogr. C47, 1358–1361. https://doi.org/10.1107/S0108270191000483.

Pasek, M.A., Lauretta, D.S., 2005. Aqueous corrosion of phosphide minerals from iron meteorites: a highly reactive source of prebiotic phosphorus on the surface of the early Earth. Astrobiology 5, 515–535.

Rai, N., van Westrenen, W., 2013. Core-mantle differentiation in Mars. J. Geophys. Res. Planets 118, 1195–1203. https://doi.org/10.1002/jgre.20093.

Righter, K., Drake, M.J., 1996. Core formation in Earth's moon, Mars, and Vesta. Icarus 124, 513–529. https://doi.org/10.1006/icar.1996.0227.

Righter, K., Drake, M.J., Yaxley, G., 1997. Prediction of siderophile element metal-silicate partition coefficients to 20 GPa and 2800 C: the effects of pressure, temperature, oxygen fugacity, and silicate and metallic melt compositions. Phys. Earth Planet. Inter. 100, 115–134.

Righter, K., Humayun, M., Campbell, A.J., Danielson, L., Hill, D., Drake, M.J., 2009. Experimental studies of metal–silicate partitioning of Sb: implications for the terrestrial and lunar mantles. Geochim. Cosmochim. Acta 73, 1487–1504. https://doi.org/10.1016/j.gca.2008.11.042.

Righter, K., Pando, K.M., Danielson, L., Lee, C.-T., 2010. Partitioning of Mo, P and other siderophile elements (Cu, Ga, Sn, Ni, Co, Cr, Mn, V, and W) between metal and silicate melt as a function of temperature and silicate melt composition. Earth Planet. Sci. Lett. 291, 1–9. https://doi.org/10.1016/j.epsl.2009.12.018.

Righter, K., King, C., Danielson, L., Pando, K., Lee, C.T., 2011. Experimental determination of the metal/silicate partition coefficient of germanium: implications for core and mantle differentiation. Earth Planet. Sci. Lett. 304, 379–388. https://doi.org/10.1016/j.epsl.2011.02.015.

Roskosz, M., Bouhifd, M.A., Jephcoat, A.P., Marty, B., Mysen, B.O., 2013. Nitrogen solubility in molten metal and silicate at high pressure and temperature. Geochim. Cosmochim. Acta 121, 15–28. https://doi.org/10.1016/j.gca.2013.07.007.

Schmitt, W., Palme, H., Wänke, H., 1989. Experimental determination of metal/silicate partition coefficients for P, Co, Ni, Cu, Ga, Ge, Mo, and W and some implications for the early evolution of the earth. Geochim. Cosmochim. Acta 53, 173–185.

Scott, H.P., Huggins, S., Frank, M.R., Maglio, S.J., Martin, C.D., Meng, Y., Santillán, J., Williams, Q., 2007. Equation of state and high-pressure stability of Fe₃P-schreibersite: implications for phosphorus storage in planetary cores. Geophys. Res. Lett. 34, L06302. https://doi.org/10.1029/2006GL029160.

Siebert, J., Corgne, A., Ryerson, F.J., 2011. Systematics of metal-silicate partitioning for many siderophile elements applied to Earth's core formation. Geochim. Cosmochim. Acta 75, 1451–1489. https://doi.org/10.1016/j.gca.2010.12.013.

Steenstra, E.S., van Westrenen, W., 2018. A synthesis of geochemical constraints on the inventory of light elements in the core of Mars. Icarus 315, 69–78. https://doi.org/10.1016/j.icarus.2018.06.023.

Steenstra, E.S., Sitabi, A.B., Lin, Y.H., Rai, N., Knibbe, J.S., Berndt, J., Matveev, S., van Westrenen, W., 2017. The effect of melt composition on metal-silicate partitioning of siderophile elements and constraints on core formation in the angrite parent body. Geochim. Cosmochim. Acta 1–48. https://doi.org/10.1016/j.gca.2017.05.034.

Stern, J.C., Sutter, B., Freissinet, C., Navarro-González, R., McKay, C.P., Archer Jr., P.D., Buch, A., Brunner, A.E., Coll, P., Eigenbrode, J.L., Fairen, A.G., Franz, H.B., Glavin, D.P., Kashyap, S., McAdam, A.C., Ming, D.W., Steele, A., Szopa, C., Wray, J.J., Martín-Torres, F.J., Zorzano, M.-P., Conrad, P.G., Mahaffy, P.R., the MSL Science Team, 2015. Evidence for indigenous nitrogen in sedimentary and aeolian deposits from the Curiosityrover investigations at Gale crater, Mars. Proc. Natl. Acad. Sci. 112, 4245–4250. https://doi.org/10.1126/science.1111863.

Stewart, A.J., Schmidt, M.W., 2007. Sulfur and phosphorus in the Earth's core: the Fe-P-S system at 23 GPa. Geophys. Res. Lett. 34, L13201. https://doi.org/10.1029/2007GL030138.

Susaki, J., Akaogi, M., Akimoto, S.-I., Shimomura, O., 1985. Garnet-perovskite transition in CaGeO₃: in-situ X-ray measurements using synchrotron radiation. Geophys. Res. Lett. 12, 729–732.

Taylor, G.J., 2013. The bulk composition of Mars. Chemie Der Erde - Geochemistry 73 (4), 401–420. https://doi.org/10.1016/j.chemer.2013.09.006.

Treiman, A.H., Jones, J.H., Drake, M.J., 1987. Core formation in the shergottite parent body and comparison with the earth. J. Geophys. Res. 92, E627–E632. https://doi.org/10.1029/JB092iB04p0E627.

Wänke, H., Dreibus, G., 1988. Chemical composition and accretion history of terrestrial planets. Philos. Trans. R. Soc. A Math. Phys. Eng. Sci. 325, 545–557. https://doi.org/10.1098/rsta.1988.0067.

Westheimer, F.H., 1987. Why nature chose phosphates. Science 235, 1173–1178. https://doi.org/10.1126/science.2434996.

van Westrenen, W., Van Orman, J.A., Watson, H., Fei, Y., Watson, E.B., 2003. Assessment of temperature gradients in multi-anvil assemblies using spinel layer growth kinetics. Geochem. Geophys. Geosyst. 4, 1–10. https://doi.org/10.1016/S0016-7037(02)00827-X.

Yagi, T., Akaogi, M., Shimomura, O., Suzuki, T., Akimoto, S.-I., 1987. In situ observation of the olivine-spinel phase transformation in $Fe_2SiO_4$ using synchrotron radiation. J. Geophys. Res. Solid Earth 92, 6207–6213. https://doi.org/10.1029/JB092iB07p06207.

Zhang, J., Li, B., Utsumi, W., Liebermann, R.C., 1996. In situ X-ray observations of the coesite-stishovite transition; reversed phase boundary and kinetics. Phys. Chem. Miner. 23, 1–10.